

Surface acoustic-wave propagation near the spin-reorientation phase transitions of ErFeO_3

G. Gorodetsky and S. Shaft

Department of Physics, Ben-Gurion University of the Negev, Beer-Sheva, Israel

(Received 25 September 1979; revised manuscript received 14 October 1980)

Experimental and theoretical results of surface acoustic-wave (SAW) propagation near the spin-reorientation region of ErFeO_3 are presented. Velocity measurements of SAW were carried out at zero field and at various magnetic fields, applied in the reorientation plane. The SAW results, in comparison with various bulk measurements, exhibit a slightly narrower reorientation temperature region. An applied magnetic field suppresses the SAW velocity at the reorientation region and shifts the transition temperatures. The same effects were previously observed for longitudinal bulk waves propagating along the c axis of the crystal. The observed results are accounted for by using phenomenological magnetic and magnetoelastic free-energy expressions in the coupled equations of motion. It is concluded that the SAW interacts with antiferromagnetic modes of the bulk. The difference between the SAW and the bulk-wave results is attributed to the effect of the surface boundary on the magnetic anisotropy.

I. INTRODUCTION

Surface acoustic waves (SAW) were recently employed in the study of phase transition.¹⁻³ The penetration of SAW into the solid bulk is of the order of one wavelength⁴ and in fact the SAW probes the near surface effects. It is known⁵ that in the absence of a coupling to critical fluctuations or excitations localized near the surface, e.g., a surface spin wave, the propagation modes of SAW can be exactly calculated from the elastic data of the bulk. On the other hand, it was found^{4,6} that the critical behavior near the surface does not exactly reflect the characteristic criticality of the bulk. This is expected in the region where the coherence length of the order parameter exceeds the dimensions of the SAW wavelength.

The objective of this work is to study the effect of a surface boundary on the nature of the spin-reorientation phase transitions in ErFeO_3 . Such a reorientation is usually associated with a relatively large coherence length,⁷⁻⁹ and in this respect it is well suited for the study of the near-surface critical behavior.

The compound ErFeO_3 in conformity with other rare-earth orthoferrites¹⁰ has a predominant antiferromagnetic spin structure of the Fe^{3+} ions. A characteristic feature of this compound is the appearance of weak ferromagnetism resulting from a small canting of the Fe^{3+} sublattice magnetizations from the antiferromagnetic axis. At room temperature the antiferromagnetic axis coincides with the orthorhombic a axis of the crystal. Upon cooling, below $T_u = 96.6$ K the magnetically ordered system rotates continuously in the $(a-c)$ plane until the antiferromagnetic axis coincides with the c axis at $T_l = 87$ K.⁸ The spin rotation is driven by competing twofold and fourfold anisotropy terms.¹¹ Associated with the rotation are two second-order displacive-type phase transitions, at T_u and T_l .⁹

Previous studies^{8,9,12-14} of sound propagation in the bulk near the reorientation region show that the magnetoelastic interactions manifest themselves by a gradual softening of the elastic constant C_{55} and by abrupt changes in C_{33} and C_{11} at T_l and T_u . It was also shown that an external magnetic field applied in the $(a-c)$ plane shifts the transition temperatures and suppresses the changes in the elastic constants. The comparison between bulk waves and SAW is possible for various propagation modes. In our experiment, for example, the SAW propagates on the $(a-c)$ plane and along the c axis of the crystal (see Fig. 1). It is shown in Sec. III that for such a configuration the SAW and the longitudinal bulk wave couple with the magnetic spin system through similar magnetoelastic coupling terms. In fact similar characteristic velocity changes were observed for the SAW and the longitudinal bulk wave propagating along the c axis.

The experimental results of SAW propagation at zero field and at various magnetic fields applied in the $(a-c)$ plane are presented in Sec. II; we also describe the experimental procedure for the excitation of SAW. The analysis of the results and the discussion are given in Sec. III.

II. EXPERIMENT AND RESULTS

The SAW measurements were carried out on a single crystal of ErFeO_3 , previously used by Gorodetsky and Luthi⁸ in their bulk-wave studies. The crystal was cut parallel to its orthorhombic $(a-c)$ plane and then polished carefully, first with alumina powder and finally with a chemical etchant. It is believed that the final chemical etching avoids the formation of strains at the polished surface. A piezoelectric ZnO layer of about $3 \mu\text{m}$ thick was sputtered on the surface and examined by x-ray diffraction and a scanning electron microscope.

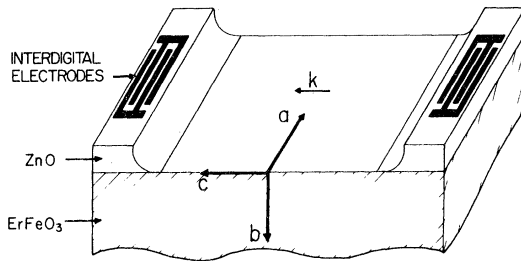


FIG. 1. Schematic description of the experimental configuration. The crystallographic axes of the crystal are a , b , and c . The SAW propagation vector \vec{k} is directed along the c axis.

It was found that the ZnO is oriented adequately¹⁵ for the excitation of SAW, i.e., the c axis of the ZnO crystallites is perpendicular to the surface. Interdigital (ID) transducers 7 mm apart from each other were fabricated by a photolithographic lift-off technique.¹⁶ A schematic description of the ID transducers, oriented for SAW propagation along the orthorhombic c axis of the ErFeO₃ crystal, is given in Fig. 1. Each one of the ID transducers consists of eight equally spaced Al electrode pairs with an aperture of 2.2 mm. The width of each electrode and the distance between adjacent electrodes is $\frac{1}{4}\lambda = 12.5 \mu\text{m}$. This configuration corresponds to a basic SAW wavelength of $\lambda = 50 \mu\text{m}$. In order to enable propagation of SAW on the free surface of the crystal, we etched off the ZnO in between the ID transducers. The crystal was mounted in a copper block to assure a uniform temperature over the entire surface. The temperature was measured with an

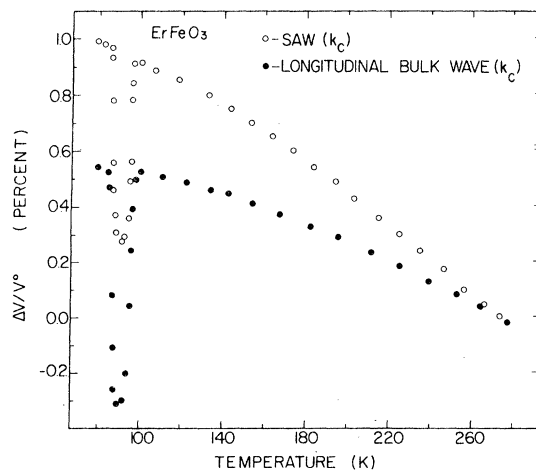


FIG. 2. Temperature dependence of the relative velocity changes of a 66-MHz SAW and a 30-MHz longitudinal bulk wave between 75 and 300 K. V^0 is the sound velocity at $T = 300$ K.

Au-0.7 at. % Fe vs Chromel thermocouple, attached to the crystal. The temperature resolution in our experiments was better than 0.04 K.

Velocity measurements of SAW were carried out by a phase comparison single-echo technique.¹⁷ Since the triple-transit echo was highly attenuated the measurements were carried out on the single-transit echo, with a resolution of ~ 100 ppm. The absolute SAW velocity at room temperature is $V^0 = (3 \pm 0.3) \times 10^5$ cm/sec. The experimentally observed velocity shifts of a 66-MHz SAW and a 30-MHz longitudinal bulk wave, propagating along the c axis in the temperature region 75–300 K, are presented in Fig. 2. Both waves exhibit marked velocity shifts at the upper and lower transition temperatures, which are superimposed on the normal elastic behavior of the crystal. The slope of each normal curve at the transition region is considered as a baseline for the magnetoelastic effects. For SAW the slope is $a = 3.6 \times 10^{-3}$ percent/K, and for the longitudinal bulk wave $a = 1. \times 10^{-3}$ percent/K. The net magnetoelastic effects for the SAW and bulk wave are shown in Fig. 3. It was found that the transition region for SAW is narrower by ~ 0.7 K than that observed for the bulk wave. The SAW transition temperatures are $T_u = 96.6$ K and $T_l = 87.7$ K. The SAW velocity shifts are smaller by 18% than those obtained for the bulk wave. A velocity dip was obtained in the SAW measurements at $T \approx 86.3$ K (see Fig. 3). Although the appearance of the dip is not fully understood, it could result from spurious reflections of bulk waves. It is important to note that this velocity dip appears at the region of the transition temperature of the bulk wave.

The net magnetoelastic effects for 198-MHz

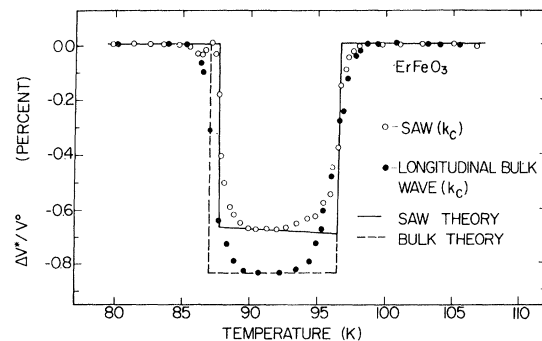


FIG. 3. Relative velocity changes with respect to the normal elastic behavior of a 66-MHz SAW and a 30-MHz longitudinal bulk wave propagating along the c axis. In this figure $\Delta V^* = \Delta V - a\Delta T$. Here ΔV is the measured velocity change. For SAW the slope of the normal elastic behavior is $a = 3.6 \times 10^{-3}$ percent/K, and for the longitudinal bulk wave $a = 1. \times 10^{-3}$ percent/K. V^0 is the sound velocity at $T = 300$ K.

SAW and a 30-MHz longitudinal bulk wave in the presence of various magnetic fields applied along the crystallographic a axis are shown in Fig. 4. An additional field of 0.5 kOe was applied in the c direction in order to obtain a reorientation of a single domain. The bulk-wave results shown in Fig. 4 were reproduced from previous measurements carried out on the same crystal by Gorodetsky *et al.*⁹ It is found that the applied magnetic fields shift the lower SAW transition temperature towards higher temperatures by 0.3 K/kOe and suppress the velocity changes at the upper transition temperatures. The SAW measurements in the presence of applied magnetic fields exhibit the same narrowing with respect to the bulk-wave data. No dispersive behavior was found at the SAW frequencies 66 and 198 MHz.

Some of our preliminary experiments were carried out prior to the etching of the ZnO overlay between the transducers. The results obtained in those experiments exhibit sporadic and nonreproducible velocity changes.

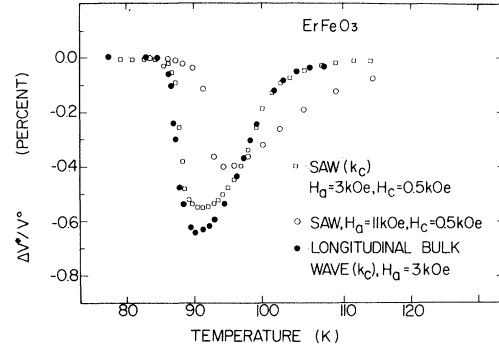


FIG. 4. Relative velocity changes with respect to the normal elastic behavior of a 198-MHz SAW and a 30-MHz longitudinal bulk wave at the spin-reorientation region. External magnetic fields are applied along the a and c axes of the crystal. In this figure $\Delta V^* = \Delta V - a\Delta T$; ΔV is the measured velocity change. For SAW the slope of the normal elastic behavior is $a = 3.6 \times 10^{-3}$ percent/K, and for the longitudinal bulk wave $a = 1 \times 10^{-3}$ percent/K. V^0 is the sound velocity at $T = 300$ K.

III. ANALYSIS AND DISCUSSION

The free-energy density F of the magnetically ordered system consists of magnetic, magnetoelastic, and elastic terms

$$F = F_m + F_{me} + F_e, \quad (1)$$

where F_m is the magnetic energy density, F_{me} represents the magnetoelastic coupling terms, and F_e is the elastic energy density. The expression for the magnetic energy density is^{14,18}

$$\begin{aligned} F_m = & E(\alpha_{1x}\alpha_{2x} + \alpha_{1y}\alpha_{2y} + \alpha_{1z}\alpha_{2z}) - D(\alpha_{1x}\alpha_{2z} - \alpha_{2x}\alpha_{1z}) - A_{xx}(\alpha_{1x}^2 + \alpha_{2x}^2) - A_{zz}(\alpha_{1z}^2 + \alpha_{2z}^2) \\ & + \frac{1}{2}K_b(\alpha_{1x}^4 + \alpha_{2x}^4 + \alpha_{1z}^4 + \alpha_{2z}^4 - 6\alpha_{1x}^2\alpha_{1z}^2 - 6\alpha_{2x}^2\alpha_{2z}^2) \\ & - H_0[(M_0 + M_a^R)(\alpha_{1x} + \alpha_{2x})\sin\psi + (M_0 + M_c^R)(\alpha_{1z} + \alpha_{2z})\cos\psi] - \vec{h} \cdot (\vec{M}_1 + \vec{M}_2). \end{aligned} \quad (2)$$

The first and second terms in the above equation represent, respectively, the symmetric and the antisymmetric exchange coupling of the canted antiferromagnetic sublattices. Here α_{1k}, α_{2k} ($k = x, y, z$) denote the normalized components of the two sublattice magnetizations \vec{M}_1 and \vec{M}_2 , respectively (see Fig. 5). E is the symmetric exchange energy density and D is the antisymmetric exchange interaction. A_{xx} and A_{zz} are twofold magnetocrystalline anisotropy coefficients. These anisotropy terms are compatible with the orthorhombic symmetry. The last terms represent the interactions with magnetic fields. H_0 is an external magnetic field, applied in the (a - c) plane and forming an angle ψ with the crystallographic c axis. Here M_a^R and M_c^R are the magnetic polarizations of the rare-earth ions along the a axis and c axis, respectively,¹⁴ and $M_0 = |\vec{M}_1| = |\vec{M}_2|$. The effect of the demagnetization field \vec{h} is also included.

The magnetoelastic interaction terms pertinent to the geometry of our SAW experiment are¹⁹

$$\begin{aligned} F_{me} = & \epsilon_{yy}[B_{21}(\alpha_{1x}^2 + \alpha_{2x}^2) + B_{22}(\alpha_{1y}^2 + \alpha_{2y}^2) + B_{23}(\alpha_{1z}^2 + \alpha_{2z}^2)] \\ & + \epsilon_{zz}[B_{31}(\alpha_{1x}^2 + \alpha_{2x}^2) + B_{32}(\alpha_{1y}^2 + \alpha_{2y}^2) + B_{33}(\alpha_{1z}^2 + \alpha_{2z}^2)] + \epsilon_{yz}B_{44}(\alpha_{1y}\alpha_{1z} + \alpha_{2y}\alpha_{2z}), \end{aligned} \quad (3)$$

where B_{ij} are magnetoelastic coefficients, ϵ_{ij} are the components of the strain tensor given by

$$\epsilon_{yy} = \frac{\partial R_y}{\partial y}, \quad \epsilon_{zz} = \frac{\partial R_z}{\partial z}, \quad \epsilon_{yz} = \frac{\partial R_y}{\partial z} + \frac{\partial R_z}{\partial y},$$

where \vec{R} is the elastic displacement. The pertinent terms of the elastic energy density are

$$F_e = \frac{1}{2}C_{22}^0\epsilon_{yy}^2 + \frac{1}{2}C_{33}^0\epsilon_{zz}^2 + \frac{1}{2}C_{44}^0\epsilon_{yz}^2 + C_{23}^0\epsilon_{yy}\epsilon_{zz}. \quad (4)$$

Here the C_{ij}^0 denote the normal elastic constants. Since the entropy change associated with the rotation of the magnetically ordered system is negligible,²⁰ the spin entropy term is omitted from the present analysis.

The equilibrium conditions for the rotating spin systems are⁹

$$\frac{\partial F_m}{\partial \delta} = 0, \quad (5a)$$

$$\frac{\partial F_m}{\partial \theta} = 0, \quad (5b)$$

where δ is the canting angle and θ is the rotation angle defined in Fig. 5. The coupled equations of motion of the two sublattice antiferromagnetic spin system and the elastic displacements are^{8,21}

$$\frac{d\vec{M}_1}{dt} = \gamma(\vec{M}_1 \times \vec{H}_1^e), \quad (6a)$$

$$\frac{d\vec{M}_2}{dt} = \gamma(\vec{M}_2 \times \vec{H}_2^e), \quad (6b)$$

$$\rho \frac{\partial^2 R_k}{\partial t^2} = \sum_{i=1}^3 \frac{\partial}{\partial x_i} \left(\frac{\partial F}{\partial \epsilon_{ki}} \right) + \vec{M}_1 \cdot \frac{\partial \vec{H}_1^e}{\partial x_k} + \vec{M}_2 \cdot \frac{\partial \vec{H}_2^e}{\partial x_k}, \quad (6c)$$

where γ is the gyromagnetic ratio and ρ is the mass density. The effective fields \vec{H}_1^e and \vec{H}_2^e are derived from the free-energy density by

$$\vec{H}_i^e = -\nabla_{\vec{M}_i} F. \quad (7)$$

The Maxwell equations for the magnetic fields associated with the sublattice magnetizations are

$$\nabla \cdot \vec{B} = 0, \quad (8a)$$

$$\nabla \times \vec{h} = -\frac{1}{c} \frac{\partial \vec{E}}{\partial t}, \quad (8b)$$

where $\vec{B} = \vec{h} + 4\pi(\vec{M}_1 + \vec{M}_2)$, and \vec{E} is the electric field. Since the phase velocity of the SAW is smaller by five orders of magnitude than the speed of light c , the magnetostatic approximation, i.e.,

$$\frac{1}{c} \frac{\partial \vec{E}}{\partial t} = 0,$$

could be applied to Eq. (8b).²² In our experiments the SAW propagates along the c direction of the crystallographic (a - c) plane and decays exponentially into the crystal (see Fig. 1). It is therefore assumed that the crystal occupies the half-space, $y > 0$. In this geometry the dynamical variables describing the magnetoelastic surface wave have the form

$$\vec{R} = \vec{R}^0 e^{-\beta k y} e^{i(kx - \omega t)}, \quad (9a)$$

$$\vec{M}_i = \vec{M}_i^0 e^{-\beta k y} e^{i(kx - \omega t)}, \quad (9b)$$

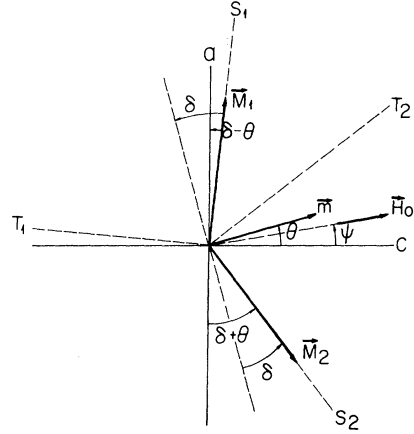


FIG. 5. Coordinates of the two sublattice magnetizations with respect to the crystallographic axes of the crystal.

$$\vec{h} = \vec{h}^0 e^{-\beta k y} e^{i(kx - \omega t)}, \quad (9c)$$

where β is a complex decay constant, k represents the SAW wave vector, and ω its angular frequency. The displacement R_x is not coupled to R_y and R_z through the equations of motion (6c) and represents a different propagation mode, which is beyond the scope of the present analysis. Also from Eqs. (8b) and (9c) we find that $h_x = 0$, $h_z = (i/\beta)h_y$, and, therefore, \vec{h} has only one independent component.

It is convenient to solve the equations of motion in coordinates of the two antiferromagnetic sublattices. The coordinate system for each sublattice magnetization is presented in Fig. 5 and the transformation from the crystallographic directions is given by the following equations¹⁸:

$$\begin{aligned} \alpha_{1z} &= S_1 \sin(\delta - \theta) - T_1 \cos(\delta - \theta), \\ \alpha_{2z} &= S_2 \sin(\delta + \theta) + T_2 \cos(\delta + \theta), \\ \alpha_{1x} &= S_1 \cos(\delta - \theta) + T_1 \sin(\delta - \theta), \\ \alpha_{2x} &= -S_2 \cos(\delta + \theta) + T_2 \sin(\delta + \theta), \\ \alpha_{1y} &= Y_1, \\ \alpha_{2y} &= Y_2, \end{aligned} \quad (10)$$

where (S_i, T_i, Y_i) $i = 1, 2$ are the normalized components of the sublattice magnetizations in the rotating antiferromagnetic coordinate systems. The angle θ defines the orientation of the net magnetic moment $\vec{m} = (\vec{M}_1 + \vec{M}_2)$ with respect to the c axis and δ is the canting angle. To a first-order approximation, $dS_1/dt = dS_2/dt = 0$. The explicit form of F_m and F_{me} in the rotating coordinate systems is given in Appendix A. Substituting the independent dynamical variables [eqs. (9) and (10)] into the equations of motion (6)–(8) one obtains a

set of linearized homogeneous algebraic equations as follows:

$$\vec{A}\vec{X}^0 = 0, \quad (11)$$

where $X^0 = (T_1^0, Y_1^0, T_2^0, Y_2^0, h_y^0, R_y^0, R_z^0)$ stand for the amplitudes of the dynamical variables at $y=0$. The components of the matrix \vec{A} are given explicitly in Appendix B. The set of equations (11) has a nonzero solution only if the determinant of \vec{A} vanishes.

This condition provides a real polynomial of the sixth order in the decay constant β , with ω and k as parameters. Of the six complex roots only three are physically acceptable, with real parts greater than zero.^{4,22} The values of these decay constants $\beta_1, \beta_2, \beta_3$ are substituted into Eqs. (11) and the equations are then solved for the dynamical variables. For each β_i one obtains the eigenvector $(T_1^{0i}, Y_1^{0i}, T_2^{0i}, Y_2^{0i}, h_y^{0i}, R_y^{0i}, R_z^{0i})$. With these eigenvectors we construct a general solution of the equations of motion of the form

$$\vec{X} = \sum_{n=1}^3 A_n \vec{X}^{0n} e^{-\beta_n k y} e^{i(kx - \omega t)}, \quad (12)$$

where A_n are the coefficients of the linear combination. This general solution must fulfill the elastic and magnetic boundary conditions. The stress-free boundary conditions are

$$\left(\frac{\partial F}{\partial \epsilon_{yy}} \right)_{y=0} = 0, \quad (13a)$$

$$\left(\frac{\partial F}{\partial \epsilon_{yx}} \right)_{y=0} = 0. \quad (13b)$$

The magnetic boundary conditions imply that the tangential component of \vec{h} and the normal component of \vec{B} are conserved and continuous across the surface $y=0$. In the geometry of our experiment they are given by

$$\sum_{n=1}^3 A_n \left(\frac{\beta_n + 1}{\beta_n} \right) h_y^{0n} + 4\pi M_0 (Y_1^{0n} + Y_2^{0n}) = 0. \quad (14)$$

The derivation of this expression is given in Appendix C. Substituting Eq. (12) into the boundary conditions [Eqs. (13) and (14)], one obtains a set of linearized homogeneous algebraic equations of the form

$$\vec{D}\vec{A} = 0. \quad (15)$$

The components of the matrix \vec{D} are given explicitly in Appendix C. The components of the vector \vec{A} are the coefficients A_n given in Eq. (12). Equations (15) have a nonzero solution only if the complex determinant of coefficients vanishes. We em-

ployed an iterative procedure which checks the determinant of Eqs. (15) for zeroes. In this way the value of the phase velocity which corresponds to given values of ω and temperature was determined to a high accuracy. A computer program was developed in order to carry out the iterative calculations.

In the analysis of the results we assumed⁸ that $K_u = -2(A_{xx} - A_{zz})$ is linearly temperature dependent. In addition it was assumed that the canting angle δ , the fourfold anisotropy coefficient K_b , and the twofold anisotropy coefficient $A_{xx} + A_{zz}$ are temperature independent. The transition temperatures depend solely on the anisotropy. A best fit of the theory to the experimental results was obtained by adjusting the bulk anisotropy K_u to the spin-reorientation region measured by the SAW, i.e., $K_u = 1.3 \times 10^7 - 1.4 \times 10^5 T$ erg/cm³. The rest of the magnetic, magnetoelastic, and elastic constants used in this fit are listed in Table I. The theoretical results of the SAW velocity shifts, at zero magnetic field and at various fields applied along the a axis of the crystal are shown in Figs. 3 and 6. There is a fairly good agreement between the calculated results and the experimental data (see Figs. 3 and 4). The SAW velocity was calculated at various frequencies up to 200 MHz and no dispersive behavior was obtained. This is found to be in agreement with our experimental results.

In order to understand the difference between the bulk and the SAW results, we have examined the effect of a surface boundary on the interaction between the SAW and the spin system. It has been established^{23,24} that the magnetic anisotropy at the surface is usually different from that of the bulk and may perturb the spin system at the surface. Such a perturbation can penetrate a considerable depth into the crystal when the effective anisotropy of the bulk goes to zero. It is very likely that within the region of the perturbed spin system, the bulk soft mode and its resonant coupling with sound waves is suppressed. On the other hand SAW will interact with the bulk soft mode whenever its wavelength (namely, its penetration depth) becomes greater than the extent of the perturbed region beneath the surface.

In order to estimate the effect of the surface, we constructed a simple spin layer model (see Fig. 7) in which the surface layer ($n=0$) has a surface anisotropy different from that of the bulk and rotates at an angle θ_s . Layers 1, 2, 3, ..., etc. form a manifold which gradually approaches the bulk rotation angle θ_0 , assigned to layer n . The number of perturbed layers rotating at angles which are different from θ_0 can be estimated from the energy stored in such a "domain wall" config-

TABLE I. Various magnetic (Refs. 8 and 29), magnetoelastic (Refs. 8 and 12), and elastic bulk constants (Refs. 8 and 12) of ErFeO_3 used in the present calculations of SAW velocity.

Sublattice magnetizations	$M_0 = 440 \text{ G}$
Symmetric exchange energy	$E = 22 \times 10^8 \text{ erg/cm}^3$
Antisymmetric exchange energy	$D = 4.4 \times 10^7 \text{ erg/cm}^3$
Bulk transition temperatures	$T_l = 87 \text{ K}, T_u = 96.6 \text{ K}$
Canting angle	$\delta = 0.01 \text{ rad}$
Bulk anisotropy energy ^a : Twofold	$K_u(T) = 1.2 \times 10^7 - 1.3 \times 10^5 T \text{ erg/cm}^3$
Fourfold	$K_b = 7.7 \times 10^4 \text{ erg/cm}^3$
Density	$\rho = 8.07 \text{ g/cm}^3$
Magnetic polarization of the rare-earth ions ^b	$M_a^R = 77.5 \text{ G}$
Gyromagnetic ratio	$\gamma = 1.86 \times 10^7 \text{ sec}^{-1} \text{ Oe}^{-1}$
Sum of twofold anisotropy coefficients	$A_{xx} + A_{zz} = 1.6 \times 10^4 \text{ erg/cm}^3$
Magnetoelastic coupling constants ^c	$ B_{31} - B_{33} = 1.2 \times 10^8 \text{ erg/cm}^3$ $ B_{21} - B_{23} = 4 \times 10^7 \text{ erg/cm}^3$ $ B_{44} = 3 \times 10^7 \text{ erg/cm}^3$
Elastic constants ^d	$C_{33}^0 = 2.76 \times 10^{12} \text{ dyn/cm}^2$ $C_{44}^0 = 1.18 \times 10^{12} \text{ dyn/cm}^2$ $C_{22}^0 = 3.6 \times 10^{12} \text{ dyn/cm}^2$ $C_{23}^0 = 1.5 \times 10^{12} \text{ dyn/cm}^2$

^a The values of the anisotropy energies in Ref. (29) were calculated from neutron diffraction data, upon assuming a linear temperature dependence of K_u . In Ref. 8 the anisotropy coefficients were arbitrarily adjusted for the transition temperatures.

^b The magnetic polarization of the rare-earth ions was calculated from the field-dependent shift of the transition temperatures.

^c The magnetoelastic coupling constants were adjusted for the anisotropy values given in this table.

^d The elastic constant C_{33}^0 is an estimated value, and was determined from the value of C_{23} of similar materials.

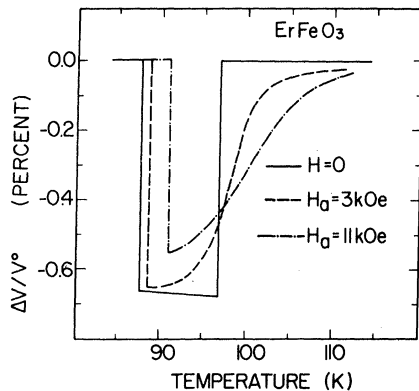


FIG. 6. Calculated velocity changes of SAW at the spin-reorientation region with external magnetic fields applied along the a axis of the crystal and at zero external field.

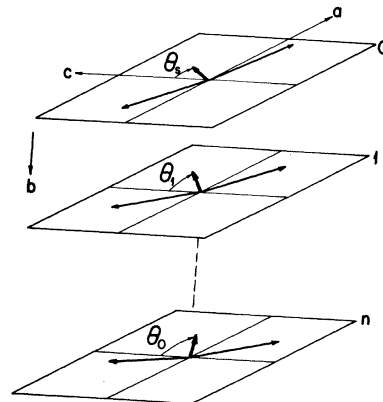


FIG. 7. Schematic description of the layer model. The long arrows describe the antiferromagnetic sublattices in each layer and the small arrows describe the spontaneous magnetization in each layer.

uration²⁵:

$$\gamma = \int_0^\infty \left[\frac{1}{2}E \left(\frac{\partial \theta}{\partial n} \right)^2 + \frac{1}{2}K_u \cos 2\theta + K_b \cos 4\theta \right] dn. \quad (16)$$

Here E is the symmetric exchange energy. The second and third terms in the integral represent the bulk anisotropy energy and n numbers the layers. The limits of the integral are 0 at the surface and ∞ in the bulk.

The antisymmetric exchange is neglected in the above expression. The number of perturbed layers n obtained by variational calculus²⁵ is

$$n = \left(\frac{1}{2}E \right)^{1/2} \int_{\theta_0}^{\theta_s} \left(\left| \frac{1}{2}K_u \cos 2\theta + K_b \cos 4\theta - \frac{1}{2}K_u \cos 2\theta_0 - K_b \cos 4\theta_0 \right| \right)^{-1/2} d\theta, \quad (17)$$

where the temperature dependence of θ_0 is determined by the equilibrium condition $\cos 2\theta_0 = -K_u/8K_b$. This integral diverges logarithmically, but a rough estimate of n may be obtained by numerical integration over 99% of the interval $\theta_s - \theta_0$. For the sake of simplicity we assume that the spins of the surface layer have higher anisotropy and remain pinned near T_i and T_u , along the corresponding principal axis, namely, $\theta_s = 0$ or $\pi/2$. The value of n at the spin-reorientation region is very sensitive to the temperature dependence of the anisotropy; e.g., for K_u and K_b listed in Table I, n varies rapidly from divergent values at $T_i = 87$ K and $T_u = 96.6$ K to a few hundred layers when the temperature is shifted into the reorientation region by 0.1 K. Such a rapid decrease in n could suit the upper transition, where the velocity shifts of the SAW and the bulk wave almost coincide at the same temperature T_u . However, neutron scattering²⁶ and Mössbauer experiments²⁷ indicate that the angular variation of θ_0 near T_i is slower than that determined by the anisotropies listed in Table I. It could be more properly described by a quadratic temperature dependence of K_u , e.g., $K_u = 6.2 \times 10^5 - 0.82T^2$ erg/cm³ (the numerical values were chosen in conformity with the equilibrium conditions). The departure from a linear temperature dependence may be compatible with the experimental results, at least as well as the linear approximation. With this value of K_u , n varies from a divergent value at T_i to $n = 1.4 \times 10^4$ at the temperature $T = 87.7$ K, at which the SAW exhibits a velocity shift. Since the distance between adjacent layers is $\sim 3 \times 10^{-4}$ μm ,²⁸ the perturbed region beneath the crystal surface at $T = 87.7$ K is ~ 4 μm . Therefore, in the temperature range 87K–87.7K the depth of the perturbed region is comparable to the SAW penetration depth and most of the magnetoelastic effect may be screened out. The same mechanism of perturbed anisotropy may

also explain the lack of a full spin-wave softening, in the neutron diffraction experiments.²⁹ In a manner similar to the effect of the surface boundary, any perturbation in the magnetic lattice will extend itself near the phase transitions and perturb the anisotropy of many spins in the surrounding. The "condensation" of islands of different anisotropy may act to suppress the soft mode.

We have also examined the possible coupling of SAW with surface spin waves. It is known³⁰ that surface spin modes may "condense" near the surface whenever the magnetic anisotropy of the bulk decreases. A condensation of this kind was studied by Chow and Keffer,²⁴ in antiferromagnetic hematite. They found that the domain of the surface modes near the spin-flop transition exceeds 10^3 atomic layers. Using a similar model for ErFeO₃ it was found that surface ($k=0$) spin-wave modes may exist at temperatures beyond the reorientation region. The penetration depth of this mode depends on the anisotropy assigned to the surface ($n=0$) layer. Within the spin-reorientation region, the antiferromagnetic layers near the surface rotate incoherently and the surface modes are highly suppressed. It is therefore unlikely that a surface soft mode affects the SAW results within the reorientation region.

In conclusion it has been shown that SAW could be used for the study of magnetoelastic effects near the surface. SAW measurements near the spin-reorientation region of ErFeO₃ exhibit velocity shifts similar to those measured by a longitudinal bulk wave. The main differences between the results of the SAW and the bulk waves are (a) the SAW velocity shifts are slightly smaller and (b) the spin-reorientation region measured by the SAW is found to be narrower by ~ 0.7 K. The difference in the velocity shifts is attributed to additional magnetoelastic and elastic energy terms pertinent to the SAW. As to the difference in the reorientation region, it is suggested that the interaction of SAW with the soft bulk spin mode, at the temperature range 87 K–87.7 K, is screened out by magnetically perturbed antiferromagnetic layers. Finally a further study with SAW of higher frequencies will probably lead to a better understanding of the effect of the surface boundary on magnetic properties near the surface.

ACKNOWLEDGMENTS

We wish to thank Vitorio Volterra for many useful discussions. This research was supported in part by a grant from the United States–Israel, Binational Science Foundation (BSF), Jerusalem, Israel. This work was done in partial fulfillment of the Ph.D. requirements of one of the authors (S.S.).

APPENDIX A

The magnetic free-energy density F_m and the magnetoelastic free-energy density F_{me} in the rotating coordinate systems are

$$\begin{aligned}
F_m = & (S_1 S_2 + T_1 T_2)(-E \cos 2\delta - D \sin 2\delta) + E Y_1 Y_2 \\
& + (S_1 T_2 - S_2 T_1)(E \sin 2\delta - D \cos 2\delta) - S_1^2 [A_{xx} \cos^2(\delta - \theta) + A_{zz} \sin^2(\delta - \theta)] \\
& - S_2^2 [A_{xx} \cos^2(\delta + \theta) + A_{zz} \sin^2(\delta + \theta)] - T_1^2 [A_{xx} \sin^2(\delta - \theta) + A_{zz} \cos^2(\delta - \theta)] \\
& - T_2^2 [A_{xx} \sin^2(\delta + \theta) + A_{zz} \cos^2(\delta + \theta)] - S_1 T_1 [(A_{xx} - A_{zz}) \sin 2(\delta - \theta)] \\
& + S_2 T_2 [(A_{xx} - A_{zz}) \sin 2(\delta + \theta)] \\
& + \frac{1}{2} K_b [(S_1^4 + T_1^4 - 6S_1^2 T_1^2) \cos 4(\delta - \theta) + (S_2^4 + T_2^4 - 6S_2^2 T_2^2) \cos 4(\delta + \theta) \\
& \quad + 4S_1 T_1 (S_1^2 - T_1^2) \sin 4(\delta - \theta) - 4S_2 T_2 (S_2^2 - T_2^2) \sin 4(\delta + \theta)] \\
& - (M_0 + M_a^R) H_0 \sin \psi [S_1 \cos(\delta - \theta) + T_1 \sin(\delta - \theta) - S_2 \cos(\delta + \theta) + T_2 \sin(\delta + \theta)] \\
& - (M_0 + M_c^R) H_0 \cos \psi [S_1 \sin(\delta - \theta) - T_1 \cos(\delta - \theta) + S_2 \sin(\delta + \theta) + T_2 \cos(\delta + \theta)] \\
& - M_0 [Y_1 h_{y_1} + S_1 h_{s_1} + T_1 h_{t_1} + Y_2 h_{y_2} + S_2 h_{s_2} + T_2 h_{t_2}], \tag{A1}
\end{aligned}$$

$$\begin{aligned}
F_{me} = & [\epsilon_{yy}(B_{21} - B_{23}) + \epsilon_{zz}(B_{31} - B_{33})][S_1 T_1 \sin 2(\delta - \theta) + S_2 T_2 \sin 2(\delta + \theta)] \\
& + (\epsilon_{yy} B_{21} + \epsilon_{zz} B_{31})[T_1^2 \sin^2(\delta - \theta) + T_2^2 \sin^2(\delta + \theta) + S_1^2 \cos^2(\delta - \theta) + S_2^2 \cos^2(\delta + \theta)] \\
& + (\epsilon_{yy} B_{23} + \epsilon_{zz} B_{33})[T_1^2 \cos^2(\delta - \theta) + T_2^2 \cos^2(\delta + \theta) + S_1^2 \sin^2(\delta - \theta) + S_2^2 \sin^2(\delta + \theta)] \\
& + (\epsilon_{yy} B_{22} + \epsilon_{zz} B_{32})(Y_1^2 + Y_2^2) \\
& + \epsilon_{yz} B_{44}[Y_1 S_1 \sin(\delta - \theta) - Y_1 T_1 \cos(\delta - \theta) + Y_2 S_2 \sin(\delta + \theta) + Y_2 T_2 \cos(\delta + \theta)]. \tag{A2}
\end{aligned}$$

Here h_x , h_y , and h_z are the components of the demagnetization field in the rotating coordinate systems.

APPENDIX B

The explicit form of Eq. (11) is

$$\begin{bmatrix} \frac{i\omega M_0}{\gamma} & A_{12} & 0 & E & -M_0 & A_{16} & A_{17} \\ A_{21} & \frac{i\omega M_0}{\gamma} & A_{23} & 0 & A_{25} & A_{26} & A_{27} \\ 0 & E & \frac{i\omega M_0}{\gamma} & A_{34} & -M_0 & A_{36} & A_{37} \\ A_{23} & 0 & A_{43} & \frac{i\omega M_0}{\gamma} & A_{45} & A_{46} & A_{47} \\ A_{51} & A_{52} & A_{53} & A_{52} & 1 - \beta^2 & 0 & 0 \\ A_{61} & A_{16} & A_{63} & A_{36} & 0 & A_{66} & A_{67} \\ A_{71} & A_{17} & A_{73} & A_{37} & 0 & A_{67} & A_{77} \end{bmatrix} \begin{bmatrix} T_1^0 \\ Y_1^0 \\ T_2^0 \\ Y_2^0 \\ h_y^0 \\ R_y^0 \\ R_z^0 \end{bmatrix} = 0.$$

Here

$$\begin{aligned}
A_{12} = & E \cos 2\delta + D \sin 2\delta + 2[A_{xx} \cos^2(\delta - \theta) + A_{zz} \sin^2(\delta - \theta)] + 2K_b \cos 4(\delta - \theta) \\
& + H_0 [(M_0 + M_a^R) \sin \psi \cos(\delta - \theta) + (M_0 + M_c^R) \cos \psi \sin(\delta - \theta)], \\
A_{16} = & ikB_{44} \sin(\delta - \theta) \quad A_{17} = -\beta k B_{44} \sin(\delta - \theta), \\
A_{21} = & -E \cos 2\delta - D \sin 2\delta + 8K_b \cos 4(\delta - \theta) - 2(A_{xx} - A_{zz}) \cos 2(\delta - \theta) \\
& - H_0 [(M_0 + M_a^R) \sin \psi \cos(\delta - \theta) + (M_0 + M_c^R) \cos \psi \sin(\delta - \theta)], \\
A_{23} = & E \cos 2\delta + D \sin 2\delta, \quad A_{25} = iM_0 \cos(\delta - \theta) / \beta,
\end{aligned}$$

$$\begin{aligned}
A_{26} &= \beta k(B_{21} - B_{23}) \sin 2(\delta - \theta), \quad A_{27} = -ik(B_{31} - B_{33}) \sin 2(\delta + \theta), \\
A_{34} &= E \cos 2\delta + D \sin 2\delta + 2[A_{xx} \cos^2(\delta + \theta) + A_{zz} \sin^2(\delta + \theta)] - 2K_b \cos 4(\delta + \theta) \\
&\quad + H_0[(M_0 + M_c^R) \cos \psi \sin(\delta + \theta) - (M_0 + M_a^R) \sin \psi \cos(\delta + \theta)], \\
A_{36} &= ikB_{44} \sin(\delta + \theta), \quad A_{37} = -\beta k B_{44} \sin(\delta + \theta), \\
A_{43} &= -E \cos 2\delta - D \sin 2\delta - 2(A_{xx} - A_{zz}) \cos 2(\delta + \theta) + 8K_b \cos 4(\delta + \theta) \\
&\quad + H_0[(M_0 + M_a^R) \sin \psi \cos(\delta + \theta) - (M_0 + M_c^R) \cos \psi \sin(\delta + \theta)], \\
A_{45} &= -iM_0 \cos(\delta + \theta)/\beta, \quad A_{46} = -\beta k(B_{21} - B_{23}) \sin 2(\delta + \theta), \\
A_{47} &= ik(B_{31} - B_{33}) \sin 2(\delta + \theta), \quad A_{51} = -4\pi M_0 i \beta \cos(\delta - \theta), \\
A_{52} &= -4\pi M_0 \beta^2, \quad A_{53} = 4\pi M_0 i \beta \cos(\delta + \theta), \\
A_{61} &= -\beta k(B_{21} - B_{23}) \sin 2(\delta - \theta) \\
&\quad - \beta k[E \sin 2\delta - D \cos 2\delta + (A_{xx} - A_{zz}) \sin 2(\delta - \theta) - 6K_b \sin 4(\delta - \theta)], \\
A_{63} &= \beta k(B_{21} - B_{23}) \sin 2(\delta + \theta) - \beta k[-E \sin 2\delta + D \cos 2\delta - (A_{xx} - A_{zz}) \sin 2(\delta + \theta) \\
&\quad + 6K_b \sin 4(\delta + \theta)], \\
A_{66} &= \beta^2 k^2 C_{22}^0 - k^2 C_{44}^0 + \rho \omega^2, \quad A_{67} = -i\beta k^2 (C_{23}^0 + C_{44}^0), \\
A_{71} &= ik(B_{31} - B_{33}) \sin 2(\delta - \theta) \\
&\quad + ik[E \sin 2\delta - D \cos 2\delta + (A_{xx} - A_{zz}) \sin 2(\delta - \theta) - 6K_b \sin 4(\delta - \theta)], \\
A_{73} &= -ik(B_{31} - B_{33}) \sin 2(\delta + \theta) \\
&\quad + ik[-E \sin 2\delta + D \cos 2\delta - (A_{xx} - A_{zz}) \sin 2(\delta + \theta) + 6K_b \sin 4(\delta + \theta)], \\
A_{77} &= \beta^2 k^2 C_{44}^0 - k^2 C_{33}^0 + \rho \omega^2.
\end{aligned}$$

APPENDIX C

The solution of Maxwell's equations (8a) and (8b) for $y > 0$ (inside the crystal) are

$$\begin{aligned}
h_x &= 0 \\
h_y &= h_y^0 e^{-\beta k y} e^{i(kz - \omega t)} \\
h_z &= -\frac{i}{\beta} h_y.
\end{aligned} \tag{C1}$$

For $y < 0$ the solutions are

$$\begin{aligned}
h_x^{\text{out}} &= 0, \\
h_y^{\text{out}} &= h_y^0 e^{ky} e^{i(kz - \omega t)}, \\
h_z^{\text{out}} &= i h_y^{\text{out}},
\end{aligned} \tag{C2}$$

Here h_y^{out} and h_z^{out} are the components of the demagnetization field outside the crystal surface. The tangential component of \vec{h} is continuous across the crystal surface; therefore

$$h_z = h_z^{\text{out}}. \tag{C3}$$

Using the above equations and Eq. (12) of the text, one obtains

$$\begin{aligned}
D_{1j} &= -k C_{22}^0 \beta_j R_y^{0j} + ik C_{23}^0 R_z^{0j} + (B_{21} - B_{23})[\sin 2(\delta - \theta) T_1^{0j} - \sin 2(\delta + \theta) T_2^{0j}] \quad (j = 1, 2, 3), \\
D_{2j} &= ik C_{44}^0 R_y^{0j} - k C_{44}^0 \beta_j R_z^{0j} + B_{44}[\sin(\delta - \theta) Y_1^{0j} + \sin(\delta + \theta) Y_2^{0j}], \\
D_{3j} &= \frac{\beta_j + 1}{\beta_j} h_y^{0j} + 4\pi M_0 (Y_1^{0j} + Y_2^{0j}).
\end{aligned}$$

$$\sum_{n=1}^3 \frac{1}{\beta_n} h_y^{0n} e^{i(kz - \omega t)} = -h_y^{\text{out}} \quad \text{at } y = 0. \tag{C4}$$

The normal component of \vec{B} is continuous across the crystal surface; therefore,

$$h_y + 4\pi M_0 (Y_1 + Y_2) = h_y^{\text{out}} \quad \text{at } y = 0. \tag{C5}$$

Using Eqs. (C4), (C5), and (12) one obtains the magnetic boundary condition

$$\sum_{n=1}^3 A_n \left[\left(\frac{\beta_n + 1}{\beta_n} \right) h_y^{0n} + 4\pi M_0 (Y_1^{0n} + Y_2^{0n}) \right] = 0 \quad \text{at } y = 0. \tag{C6}$$

All the boundary conditions [Eqs. (13a), (13b), and (C6)] form, in the linear approximation, a set of homogeneous equations of the form

$$\begin{bmatrix} D_{11} & D_{12} & D_{13} \\ D_{21} & D_{22} & D_{23} \\ D_{31} & D_{32} & D_{33} \end{bmatrix} \begin{bmatrix} A_1 \\ A_2 \\ A_3 \end{bmatrix} = 0, \tag{C7}$$

where

- ¹L. Bjerkan and K. Fossheim, in *Phonon Scattering in Solids*, Proceedings of the Second International Conference on Phonon Scattering in Solids, Nottingham, 1975, edited by L. I. Challis, V. W. Rampton, and A. F. G. Wyatt (Plenum, New York, 1976), p. 265; L. Bjerkan and K. Fossheim, *J. Phys. D* **10**, 925 (1977); *Solid State Commun.* **21**, 1147 (1977).
- ²M. Levi, H. Salvo, Jr., D. A. Robinson, K. Maki, and M. Tachiki, in *IEEE Ultrasonics Symposium Proceedings, Annapolis, 1976*, edited by J. de Klerk and B. McAvoy (IEEE, New York, 1976), p. 633.
- ³C. Lingner and B. Luthi, private communication.
- ⁴G. W. Farnell, *Physical Acoustics*, edited by Warren Mason and R. N. Thurston (Academic, New York, 1970), Vol. VI, p. 109.
- ⁵See, e.g., A. J. Slobodnik, Jr., *Proc. IEEE* **64**, 581 (1976).
- ⁶R. Kretschmer and K. Binder, *Phys. Rev. B* **20**, 1065 (1979).
- ⁷L. M. Levinson, M. Luban, and S. Shtrikman, *Phys. Rev.* **187**, 715 (1969).
- ⁸G. Gorodetsky and B. Luthi, *Phys. Rev. B* **2**, 3688 (1970).
- ⁹G. Gorodetsky, B. Luthi, and T. J. Moran, *Int. J. Magn.* **1**, 295 (1971).
- ¹⁰For a review of the magnetic properties of orthoferrites see D. Treves, *J. Appl. Phys.* **36**, 1033 (1965); R. L. White, *ibid.* **40**, 1061 (1969).
- ¹¹H. Horner and C. M. Varma, *Phys. Rev. Lett.* **20**, 845 (1968).
- ¹²A. N. Grishmanovskii, V. V. Lemanov, G. A. Smolenskii, A. M. Balbashov, and A. Ya. Chervonenkis, *Fiz. Tverd. Tela (Leningrad)* **16**, 1426 (1974) [*Sov. Phys.—Solid State* **16**, 916 (1974)].
- ¹³G. Gorodetsky, R. M. Hornreich, S. Shaft, B. Sharon, A. Shaulov, and B. M. Wanklyn, *Phys. Rev. B* **16**, 515 (1977).
- ¹⁴G. Gorodetsky, S. Shaft, and B. M. Wanklyn, *Phys. Rev. B* **14**, 2051 (1976).
- ¹⁵For a review of ZnO thin-film surface-wave transducers, see Fred. S. Hickernell, *Proc. IEEE* **64**, 631 (1976).
- ¹⁶For a review of photolithographic techniques and their applications to SAW see Henry I. Smith, *Proc. IEEE* **62**, 1361 (1974).
- ¹⁷T. J. Moran and B. Luthi, *Phys. Rev.* **187**, 710 (1969).
- ¹⁸F. B. Hagedorn and E. M. Gyorgy, *Phys. Rev.* **174**, 540 (1968).
- ¹⁹W. I. Dobrov, *Phys. Rev.* **134**, A734 (1964).
- ²⁰A. Berton and B. Sharon, *J. Appl. Phys.* **39**, 1367 (1968).
- ²¹R. L. Melcher and D. I. Bolef, *Phys. Rev.* **186**, 491 (1969).
- ²²R. Q. Scott and D. L. Mills, *Phys. Rev. B* **15**, 3545 (1977).
- ²³See, e.g., H. T. Quach, A. Friedmann, C. Y. Wu, and A. Yelon, *Phys. Rev. B* **17**, 312 (1978); G. T. Rado, *ibid.* **18**, 6160 (1978).
- ²⁴H. Chow and F. Keffer, *Phys. Rev. B* **10**, 243 (1974).
- ²⁵See, e.g., Soshin Shikazumi, *Physics of Magnetism* (Wiley, New York, 1964).
- ²⁶H. Pinto, G. Shachar, H. Shaked, and S. Shtrikman, *Phys. Rev. B* **3**, 3861 (1971).
- ²⁷R. W. Grant and S. Geller, *Solid State Commun.* **7**, 1291 (1969).
- ²⁸M. Eibschutz, *Acta Crystallogr.* **19**, 337 (1965).
- ²⁹S. M. Shapiro, J. D. Axe, and J. P. Remeika, *Phys. Rev. B* **10**, 2014 (1974).
- ³⁰See, e.g., J. C. S. Levy and Diep-The-Hung, *Phys. Rev. B* **18**, 3593 (1978).